A Swirler Stabilized Combustion Chamber for a Micro-Gas Turbine Fuelled with Natural Gas

Guenther C. Krieger
guenther@usp.br
University of São Paulo
Department of Mechanical Engineering
05508-900 São Paulo, SP, Brazil

André P. V. de Campos
andre.perpignan.campos@usp.br
University of São Paulo
Department of Mechanical Engineering
05508-900 São Paulo, SP, Brazil

Fernando L. Sacomano Filho
fernando.sacomano@gmail.com
University of São Paulo
Department of Mechanical Engineering
05508-900 São Paulo, SP, Brazil

Rafael C. de Souza
rafael.cavalcanti.souza@gmail.com
University of São Paulo
Department of Mechanical Engineering
05508-900 São Paulo, SP, Brazil

Micro-gas turbines are a good alternative for on-site power generation, since their operation is very reliable. The possibility of operating with various fuels increases versatility and, as a result, the usage of these devices. Focusing on a performance improvement of a tri-fuel low-cost micro-gas turbine, this work presents investigations of the inner flow of its combustion chamber. The aim of this analysis was the characterization of the flame structure by the temperature field of the chamber inner flow. The chamber was fuelled with natural gas. In the current chamber, a swirler and a reversed flow configuration were utilized to provide flame stabilization. The inner flow investigations were done with numerical analysis, which were compared to experimental data. The analysis of the inner flow was done with numerical simulations, which used the RSM turbulence model. A β-PDF equilibrium model was adopted to account for the turbulent combustion process. Different models of heat transfer were compared. Thermal radiation and specially heat conduction in the liner walls played significant roles on results.
Keywords: *swirler stabilization, natural gas, equilibrium combustion model*

Introduction

Gas turbines are one of the most reliable devices for power generation, as they do not depend on environmental conditions and are able to operate on demand. Within this class of devices, micro-gas turbines have the advantage of being used in on-site generation. This kind of usage is important for areas where the costs to distribute power are high or for customers that need an independent and reliable energy source.

The combustion chamber is the gas turbine component responsible for receiving the combustion process that provides energy to the turbine section. The main challenges faced in the combustion chamber design are related to wall cooling, flame stability and emissions control (Lefebvre and Ballal, 2010). These features determine gas turbine operational range, durability, cost and emissions characteristics.

This work presents an analysis on a low cost micro-gas turbine combustion chamber able to operate with natural gas, LPG and ethanol. The objective is to contribute to the development of technology and solutions demanded by the on-site generation.

The micro turbine combustion chamber configuration has changed as its development evolved. Straight flow chamber with and without dilution holes, as well as bluff body stabilized flames were adopted, until the reversed flow configuration with swirler stabilized flames provided the best operational conditions. All these combustor types are adequate for use in single shaft micro gas turbines, as reported in literature.

Tuccillo and Cameretti (2005), and Cameretti, Reale and Tuccillo (2007) give a comprehensive view on micro gas turbines combustion chambers. A literature review on combustor design was conducted by Tuccillo and Cameretti (2005), discussing design strategies and the different possible geometries. In addition, they also present a numerical study of three classes of combustors (diffusion annular, lean pre-mixed and Rich burn-Quick quench-Lean burn), where the flame stabilization was reached using a swirler.

Paper received 15 February 2012. Paper accepted 21 June 2012
Technical Editor: Luís Fernando Silva

Tomczak et al. (2002) describe the studies carried out on an industrial gas turbine combustor fed with mixtures of natural gas and hydrogen. CFD studies using a commercial code were performed changing fuel composition from natural gas to pure hydrogen. The main goal of the numerical simulations was to predict the internal and the wall temperature distribution as well as combustion phenomena. The flame is stabilized by a combination of swirler air and the formation of recirculation zones. The 3D-calculation was based on mixture fraction and chemical equilibrium model. The authors argued that this approach has an additional benefit of allowing a more accurate estimation of the flow field mean density than using the finite rate formulation (Fluent Inc., 2000). No heat transfer effects were taken into account. This approach is similar to the No Heat Transfer model used in this work. The comparison between measured and calculated data is evaluated based on the wall temperatures using pure natural gas or pure hydrogen. The overall agreement of the wall temperature is good.

Khelil et al. (2009) presented the numerical prediction of a high swirling non-premixed confined natural gas diffusion flame in order to predict the pollutant NOx emissions using the PDF model coupled with the Reynolds stress model (RSM). A chemical equilibrium model in conjunction with the assumed shape of the PDF is adopted. The mixture fraction PDF is described with a β-function. In order to predict the NOx emissions, a NOx post-processor of the Fluent has been performed. The concentration of O and OH radicals is obtained assuming the partial-equilibrium and using a PDF in terms of temperature. The numerical simulation of various factors influencing the combustion process are examined and compared favorably with experimental results. This model is very similar to the combustion model used in this work.

Ghenai (2010) reports the numerical investigation of the combustion of syngas fuel mixture in gas turbine can combustor. The objective is to understand the impact of the variability in the alternative fuel composition and heating value on combustion performance and emissions. The composition of the fuel burned in can combustor was changed from natural gas (methane) to syngas fuel with hydrogen to carbon monoxide (H2/CO). The mathematical models used for syngas fuel combustion consist of the k-ε model for

turbulent flow, mixture fraction and presumed Probability Density Function (PDF) approach for non-premixed gas combustion. Radiative heat transfer in the flame is accounted for with the P-1 radiation model (Modest, 2003). No comparison with experimental data is done. Instead, the maximum temperature for the methane combustion is compared to the adiabatic flame temperature to validate the whole numerical model. The temperature deviations were lower than 2%, so that the model was considered validated.

The present work addresses numerical simulations and experimental evaluations of the mentioned combustion chamber operating with natural gas. The main objective of these investigations was to increase the understanding on the flow behavior inside this proposed combustion chamber configuration. Numerical simulations were done to provide information about some operational details regarding the chamber, observing the stabilization zone provided by the swirler and the influences of different heat transfer forms inside the chamber. Experimental data was used to guide numerical simulations modeling and also to analyze the performance of the entire device.

Nomenclature

A = *absorption coefficient*
f = *mixture fraction*
h = *enthalpy*
I = *radiation intensity*
$\vec{n}$ = *wall area normal vector*
P = *probability density function*
p = *pressure*
$\vec{r}$ = *position vector*
S = *source term*
$\vec{s}$ = *direction vector of the travelling radiative ray*
T = *temperature, K*
t = *time*
u = *velocity*
x = *Cartesian spatial coordinate*

Greek Symbols

ε = *emissivity*
Φ = *scattering phase function*
Ω = *solid angle*
ψ = *general quantity*
ρ = *density, kg/m^3*
σ = *Stefan-Boltzmann constant*
σ_s = *scattering coefficient*
Γ = *diffusivity*

Subscripts

b = *black body*
w = *at the wall*
ψ = *general quantity*
op = *at operating pressure*

Superscripts

~ = *density-weighted average*
- = *time average*
′ = *relative to the travelling radiative ray incident on control volume*
′′^{2} = *variance of a quantity*

Experimental Setup

The combustion chamber configuration was modified during the development of the tri-fuel low cost micro-gas turbine. The main project of the entire micro gas turbine setup has the objective to be a low cost system. In the view of this challenge, difficulties were found to design and build a stable combustion chamber. Some of these difficulties were associated with the use of a regular automotive turbo compressor as air feeding system, chosen to reduce costs. The turbo compressor does not allow the direct control of air inflow. As a result, air/fuel mixture is dynamically controlled by the flow field inside the chamber. This behavior was the main obstacle to achieve a stable combustion chamber.

The first design configurations were based on straight flow chambers with bluff bodies and, afterwards, with swirler on the primary air injection. This kind of chamber provided stable flames, but walls overheated, compromising their durability. Better results were achieved when reversed flow configuration was used. This configuration provides cooling of chamber walls, as well as pre-heating of incoming air, which enhances flame stability. Figure 1 presents a cut view of the reversed flow chamber this work studies, as well as the chamber main dimensions.

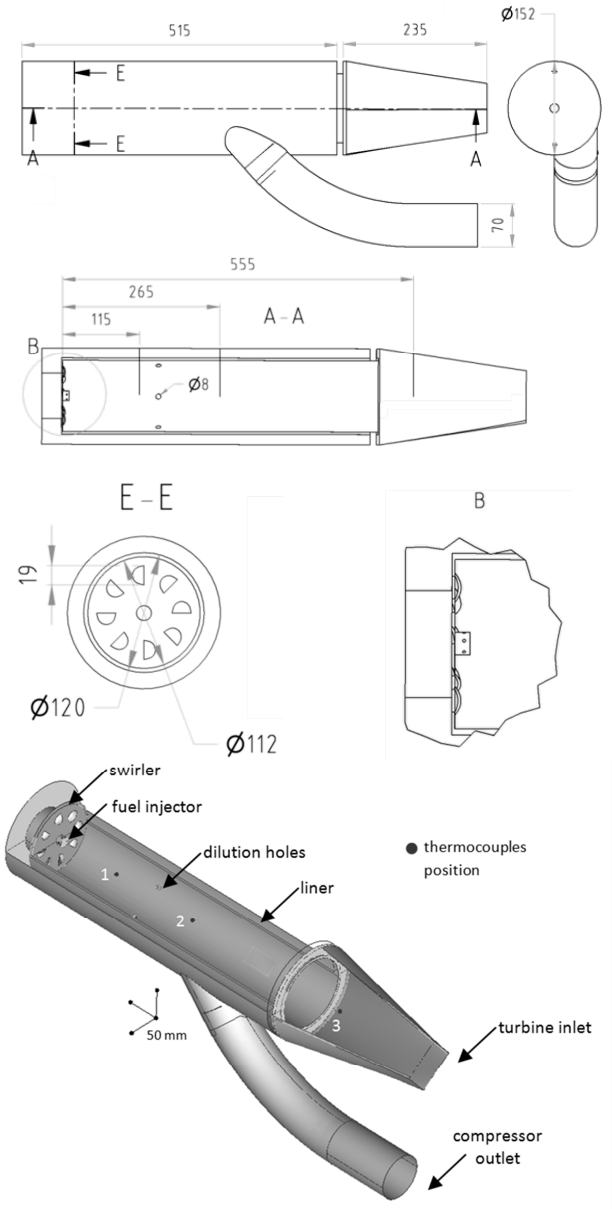

Figure 1. Geometry of the reversed flow combustion chamber.

In Fig. 1, the numbered dots represent the thermocouples' positions on the experiments. It is worth to indicate that the actual set stands on the vertical position and is turned here for better visualization.

The air inflow is made through a manifold connecting compressor outlet to the chamber case. Fuel enters the chamber through the injector located at the swirler center, as seen in Fig. 1. Injection is made radially, in a plane parallel to the swirler plane, through six equally spaced holes. Liner walls received six dilution holes with 8 mm diameter displaced radially. The experiments carried for this work used only natural gas, although the set is able to operate with LPG and ethanol.

Temperature and flow measurements were performed to allow comparison of the computational simulations to experimental results. The air mass flow entering the chamber was measured using a calibrated ASME nozzle, which is based on pressure difference, attached to the compressor inlet, as shown in the scheme of Fig. 2. Water columns indicating pressure differences had a millimeter resolution, yielding to an uncertainty of $3 \cdot 10^{-3}$ kg/s. Fuel mass flow was measured using a rotameter ($2 \cdot 10^{-4}$ kg/s of uncertainty) and the proper corrections made with measured pressure and temperature on the fuel line, taken with a manometer (0.07 kgf/cm^2 of uncertainty) and a T-type thermocouple.

Temperatures inside the chamber were measured with three N-type thermocouples inserted through holes in the chamber case. The tip of each thermocouple was located as shown in Fig. 1. Thermocouples' points in the chamber will be referred to as 1, 2 and 3. In addition, a K-type thermocouple was positioned at the turbine outlet. The uncertainties for the temperature measurements were 5 K for the N-type thermocouples, K-type thermocouples and T-type thermocouples. All uncertainties reported in this paper have 95% of confidence level.

Experiments were performed in two stable operational regimes. Regimes were determined by the fuel mass flow, manually controlled by a valve. Air flow tends to increase when fuel flow increases. Combustion stability and compressor surge are responsible for the mass flow inferior limit, while fuel line capability limits higher mass flows.

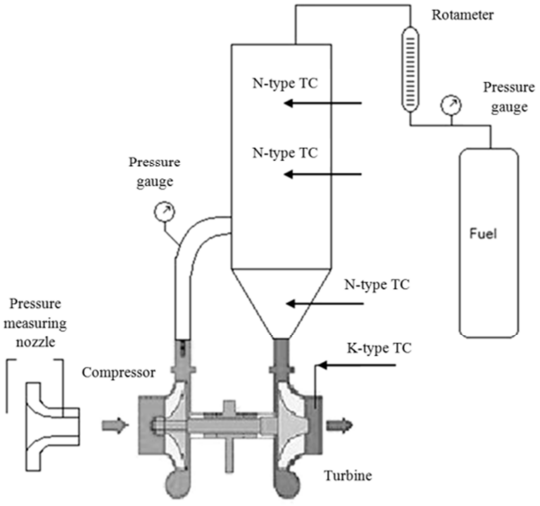

Figure 2. Experimental test rig.

The averaged values presented here were taken from various measurements performed at the same operating condition. Table 2, at the Results section, presents these mean measured data for cases 1 and 2. Mass flows averages were taken from at least three measurements performed on each configuration (case). While each measurement was taken, temperatures were acquired five times per second. Each measurement took about one minute to be performed and temperatures were taken during this time for every measurement. Fuel flow was controlled manually, while air flow depended only on the turbocompressor regime.

Mathematical and Numerical Modeling

The turbulent flow inside the combustion chamber was simulated using the commercial CFD code Ansys Fluent®, which is based on the finite volume method. A RANS based turbulence modeling was adopted. Regarding this turbulence modeling and the presence of combustion phenomenon, the Favre's averaging was used in the governing equations of transported quantities. Thus, a transport equation for a general quantity can be written as shown in Eq. (1).

$$\frac{\partial \bar{\rho}\widetilde{\psi}}{\partial t} + \frac{\partial \bar{\rho}\widetilde{\psi}\widetilde{u_j}}{\partial x_j} = + \frac{\partial}{\partial x_j}\left(\Gamma_\psi \frac{\partial \widetilde{\psi}}{\partial x_j}\right) + S_\psi \tag{1}$$

Momentum, turbulent kinetic energy, turbulent kinetic energy dissipation, Reynolds stresses $\left(\bar{\rho}\widetilde{u_i''u_j''}\right)$, enthalpy (in simulations with heat transfer), mixture fraction and mixture fraction variance were the transported quantities. The last two quantities are detailed in the next section.

The variable density flow approach with low Mach number was used. The overall flow field inside the combustion chamber has low velocities. However, a very small region had velocities higher than 0.3 Ma, due to the fuel injection. In Ansys Fluent®, the option of using a density based approach disables the non-premixed combustion modeling. Hence, considering that this work intends to model combustion as a non-premixed process, a pressure based approach was adopted. However, a compressibility correction, presented in Eq. (2), was used to account for the effects in this high velocity region.

$$\bar{\rho} = \rho_{op} \frac{\bar{p}}{p_{op}} \tag{2}$$

A velocity-pressure coupling was necessary to close the transport equations, since a pressure based approach was adopted. The SIMPLE (Semi-Implicit Method for Pressure-Linked Equations) algorithm was adopted.

Reynolds Stress Model (RSM) was used to account for turbulence effects. The option for this model was due to the swirling behavior inside the combustion chamber. This behavior requires the modeling of the anisotropic part of the Reynolds Stress tensor. This model for combustion chambers (and swirling flows as a whole) has proven to provide good results (Weber et al., 1990; Xia, 1998; and Palm, 2006). Model standard parameter values were used in the simulations.

Discretization of advective terms, second term in Eq. (1) of transport equations, was done with first order Up-wind scheme. Discretization of diffusive terms, third term in Eq. (1), was done with the central difference scheme (CDS). Time discretization was not necessary, since steady state simulations were done.

The discrete ordinate model was used to account for the influence of radiation on temperature. There is evidence that this method is adequate to correctly simulate radiation on gas turbines (Kayakol et al., 2000). The radiative transfer equation in the direction $\vec{s}$ is presented by Eq. (3). For a given direction this equation is treated numerically in the same manner as Navier-Stokes and other transport equations, as Eq. (1) (Fluent Inc., 2000).

$$\nabla \cdot (I(\vec{r},\vec{s})\vec{s}) + (a+\sigma_s) I(\vec{r},\vec{s}) = a\frac{\sigma T^4}{\pi} + \frac{\sigma_s}{4\pi}\int_0^{4\pi} I(\vec{r},\vec{s}')\,\Phi(\vec{s}\cdot\vec{s}')\,\mathrm{d}\Omega' \tag{3}$$

Considering the walls as diffuse reflecting surfaces, the boundary conditions for Eq. (3) are represented by Eq. (4). In this work, scattering factor was set to zero, so that only emission and absorption of the medium were considered. Walls were assumed to be black bodies ($\varepsilon = 1$), which is a reasonable assumption given the massive presence of soot and rust in the chamber walls (Kayakol, 2000). The black body intensity is given by the Planck distribution and is evaluated at wall temperature (Modest, 2003).

The absorption coefficient of the gas mixture was calculated with the sum of gray gases model (Modest, 2003). In this model, emissivity and absorptivity of the gas mixture is determined as a weighted sum of the water vapor and carbon dioxide absorptivity. The weight of the species can be found in the work by Modest (2003). The direction domain was discretized with 2x2 solid angles in the polar and azimuthal spherical coordinates.

$$I(\vec{r}_w, \vec{s}) = \varepsilon(\vec{r}_w) I_b(\vec{r}_w) + [1 - \varepsilon(\vec{r}_w)]/\pi \int_{\vec{n}\cdot\vec{s}<0} I(\vec{r}_w, \vec{s}') \, |\vec{n} \cdot \vec{s}| \mathrm{d}\Omega' \tag{4}$$

Combustion modeling and statistical treatment

Equilibrium combustion model for non-premixed flames was used to model chemical reactions. This model assumes that chemical reactions happen until they reach the chemical equilibrium. Even though this approach has limitations, it is adequate to predict temperature distributions in gas turbines combustion chambers (Tomczak et al., 2002; Ghenai, 2010). The equilibrium combustion model has been used extensively for turbulent non-premixes flame calculation, as can be seen on Kent and Honnery (1987), Piro (2007), and Sacomano Filho (2011). Flame instability cannot be predicted using this modeling along with the RANS approach. Once the main goal of this work is the prediction of temperature distribution and flow pattern inside the combustor, in operational regime far from instabilities, the equilibrium model can be considered as suitable.

The model requires mixture fraction transport to allow the combustion phenomenon computation in the flow field. The transport equation for its quantity is presented by Eq. (5).

$$\frac{\partial \bar{\rho}\tilde{f}}{\partial t} + \frac{\partial \bar{\rho}\tilde{f}\widetilde{u_j}}{\partial x_j} = + \frac{\partial}{\partial x_j}\left(\Gamma_f \frac{\partial \tilde{f}}{\partial x_j}\right) \tag{5}$$

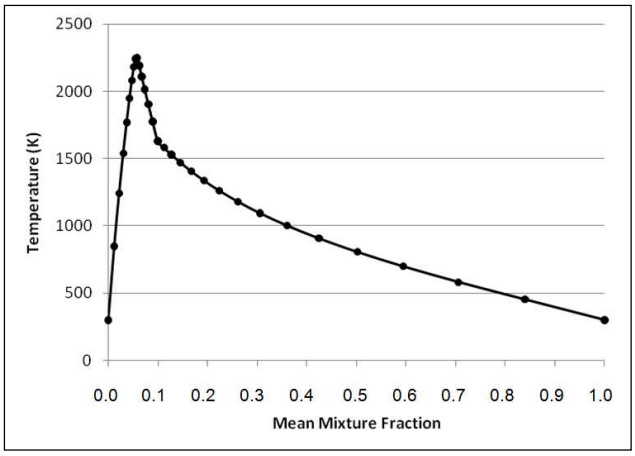

Figure 3. Temperature as a function of the mixture fraction for natural gas.

In laminar adiabatic flames, quantities as temperature, mixture density and mass fractions of chemical species can be rightly extracted from mixture fraction. Figure 3 presents the relation between mean temperature and mean mixture fraction for the natural gas reaction which, in this case, is represented by methane. Nevertheless, in turbulent flames these quantities cannot be rightly extracted from mixture fraction, since only the mean quantity is transported. In the view of this fact, a statistical treatment is done to allow dependent quantities derivation from mixture fraction.

In this work, the statistical treatment of the turbulent reaction was done with the presumed Probability Density Function (PDF) approach, specifically the β-PDF. Calculation of this presumed PDF requires the value of the local mixture fraction variance. Ansys Fluent transports the mixture fraction variance according to Eq. (6) in RANS based turbulence modeling, where C_g and C_d are parameters which have values of 2.86 and 2.0 respectively.

$$\frac{\partial \bar{\rho}\widetilde{f''^2}}{\partial t} + \frac{\partial \bar{\rho}\widetilde{f''^2}\widetilde{u_j}}{\partial x_j} = \frac{\partial}{\partial x_j}\left(\Gamma_f \frac{\partial \widetilde{f''^2}}{\partial x_j}\right) + C_g \mu_t \left(\frac{\partial \tilde{f}}{\partial x_j}\right)^2 - C_d \frac{\bar{\rho}\varepsilon}{k}\widetilde{f''^2} \tag{6}$$

A mean quantity can be calculated by the presumed PDF as presented by Eq. (7).

$$\tilde{q} = \int_{-\infty}^{\infty} q(f)\tilde{P}(f)df \tag{7}$$

The presumed PDF is given by Eq. (8).

$$\tilde{P}(f) = \frac{f^{\alpha-1}(1-f)^{\beta-1}\Gamma(\alpha+\beta)}{\Gamma(\alpha)\Gamma(\beta)} \tag{8}$$

In the case of Eq. (8), $\Gamma(\psi)$ is the gamma function and α and β parameters can be calculated as shown by Eq. (9).

$$\alpha = \tilde{f}\left[\frac{\tilde{f}(1-\tilde{f})}{\widetilde{f''^2}}\right] \text{ and } \beta = \frac{(1-\tilde{f})}{\tilde{f}}\alpha \tag{9}$$

For simulations with heat transfer, a joint-β-PDF of mixture fraction and enthalpy is used to account for the turbulent reaction treatment. In this case, the mean quantity is calculated by Eq. (10).

$$\tilde{q} = \int_{-\infty}^{\infty}\int_{-\infty}^{\infty} q(f,h)\tilde{P}(f,h)df\,dh \tag{10}$$

Boundary conditions

A plausible definition of the boundary conditions is highly important to perform simulations that actually represent real situations. Masses entering the domain received a mass flow inlet boundary treatment, at the manifold entrance and the fuel injector. This approach prescribes a constant mass flow rate and allows total pressure to fluctuate in function of the inner solution. The inflow direction was set normal to the boundary. Information on the turbulence is also required for complete boundary conditions definition. For the air inlet, turbulence intensity was set to 10% following information on compressor outlet flow (Choi and Kang, 1999) and length scale to 0.01 m according to the duct size. Mixture fraction was imposed as zero. Set fuel inlet values were 5% and 0.001 m. For the fuel, mixture fraction was set to 1.

Flow outlet entering the turbine was treated with the pressure outlet condition. In this case, a value for a static pressure on the outlet boundary must be specified. This value is relative to the operational pressure and was set to zero. Operational pressure used in all simulations had a value of 2 bar, accounting for a mean observed compressor outlet pressure. Thus, it was assumed that pressure on the turbine inlet had the same value from the compressor outlet, which was increased on the simulations due to the mass flow inlet condition. Turbulence intensity and length scale were prescribed as for the air inlet.

Grids

All the grids used in this work are unstructured and composed by tetrahedral elements. Near swirler region, inner liner walls and the region inside the liner received better refinements, comparing to those used in the inlet manifold and outlet cone. Two different meshes were employed in the simulations. One of them possesses computing nodes between liner walls, being able to account for heat conduction in this region, while the other does not.

To guarantee mesh independency, a simple test was performed. Temperature results between three different refinements were compared in the positions where thermocouples were located. These refinements (named A, B and C in Table 1) are proportional to each other, meaning that all regions were refined with a given factor.

Table 1. Numerical mesh independence.

Mesh	A	B	C
Elements	3.9 Million	4.5 Million	6.3 Million
Temperature 1(K) / Deviation	1542.7 (-)	1487.4.7 (3.58%)	1528.9 (2.79%)
Temperature 2 (K) / Deviation	888.3 (-)	921.2 (3.70%)	908.1 (1.42%)
Temperature 3 (K) / Deviation	1014.3 (-)	1028.9 (1.44%)	1022.5 (0.62%)

Simulations were performed with mass flows close to those of Case 1 (0.180 kg/s for air and 0.00361 kg/s for methane) and with no heat transfer modeling. Mesh tests were performed before the experiments and the mass flows were based on previous experiments for different chamber configurations. Due to the expensive simulation time, no further calculations were carried out with the measured mass flow rates.

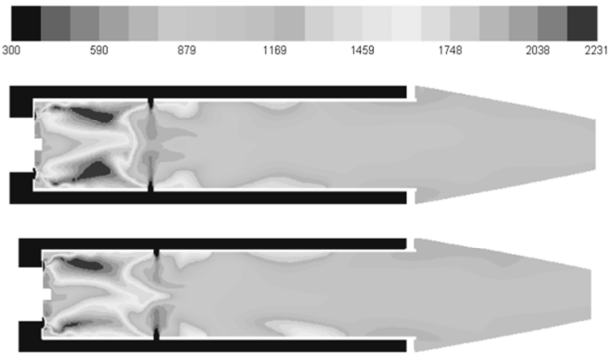

Figure 4. Mean temperature (K) contours for mesh refinements A and C with no heat transfer simulation.

Evaluating the specific points, higher deviations were found for point 1. The region where this thermocouple is positioned has the strongest gradients. The thermocouple stands at the center of the chamber, between the two high temperature areas (which are actually a tridimensional annular volume) formed before the dilution holes. Although the contours structures are very similar, any small positioning difference of these structures may greatly alter the temperatures in a given point. No great difference can be seen in Fig. 4, which compares the whole temperature fields for refinements A and C. No significant grid dependence on temperature is observed in Table 1, since the maximum deviation is 3.7%. Once the aim of this study is to understand the phenomena inside the chamber, these small variations were considered irrelevant and refinement A was adopted for all simulations.

Results and Discussion

Experimental data

Mass flows and temperatures were measured experimentally using the described apparatus. Two regimes were maintained for accomplishing the measurements. Fuel mass flow was controlled manually, while air flow depended on the resulting turbocompressor regime. Table 2 presents the average results of the measurements performed in each regime.

Table 2. Experimental conditions and mean results.

	Cases	
	1	2
Air mass flow (kg/s)	0.171	0.129
Fuel mass flow (kg/s)	$3.18(10^{-3})$	$2.22(10^{-3})$
Global equivalence ratio	0.318	0.294
Thermocouple 1 (K)	1357.4	1334.1
Thermocouple 2 (K)	1097.8	1087.1
Thermocouple 3 (K)	1113.4	1070.5
Thermocouple turbine outlet (K)	826.9	832.6

Simulations

Both cases were simulated imposing the mass flows in Table 2 to the previously described boundary conditions. Each case was firstly simulated considering two different approaches: without heat transfer (neither radiation nor conduction in the liner) and with radiation and conduction in the liner. All cases are adiabatic, since there is no heat exchange with the environment through casing walls. For comparison of the separated influences of conduction and radiation, two more heat transfer models were simulated: only radiation and solely conduction.

The main goal of this study was to compare the effect of heat transfer on the flow and temperature patterns inside the combustion chamber. By analyzing the temperature contours of the simulations without heat transfer and accounting for both radiation and conduction, as shown in Fig. 5, different structures are noticed. Temperature distributions differ more in the region close to the swirler, where the highest temperatures are found. Of course, temperatures between liner walls and the casing are also affected by the presence of heat conduction in the liner.

It is worth pointing that cases 1 and 2 had very similar profiles (see Fig. 7). This was expected, since their global equivalence ratios are close to each other.

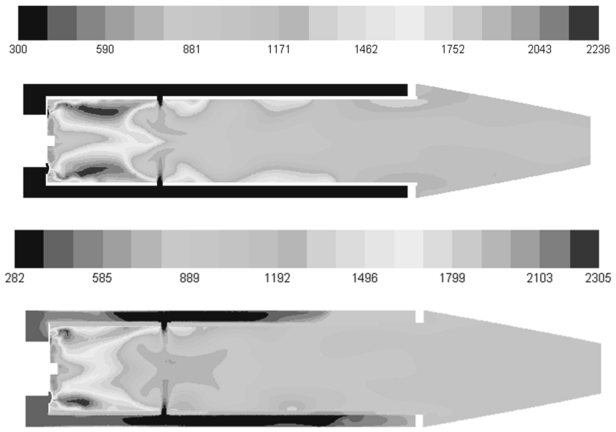

Figure 5. Mean temperature (K) contours for case 1 with no heat transfer (top) and radiation and conduction (bottom) models.

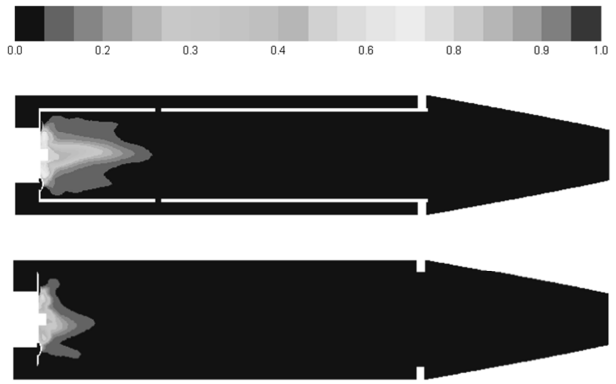

Figure 6. Mean mixture fraction contours for case 1 with no heat transfer (top) and radiation and conduction (bottom) models.

The different structures of the temperature fields noticed in Fig. 5 are explained by the fact that heat transfer alters the whole flow pattern. As a result, the mixing process is modified, as seen in Fig. 6, which shows the mean mixture fraction distribution. With no heat transfer approach, mixing elongates further from the fuel injection. As temperature is dependent on mixture fraction in the employed combustion model, they are affected.

Table 3 shows the simulations results taken from the points where thermocouples were located. Since thermocouples do not measure exactly one point and there is a small uncertainty regarding thermocouples' tips position, the temperatures shown in the table are averages of the temperatures on the computational nodes located in a 1 cm radius around the estimated thermocouples positions.

The same table also presents the deviations of the computational results to the experiments. At the location of the thermocouple 1, modeling with no heat transfer overestimated temperatures while heat transfer modeling underestimated. This is explained by the mentioned different pattern in the high temperature region. With such difference, comparisons of single points may be misleading.

Table 3. Simulation results and deviation from experiments.

		Cases	
		1	**2**
Thermocouple 1 (K) / Deviation	No heat transfer	1502.1 (+10.7%)	1415.9 (+6.1%)
	With radiation and conduction	1190.5 (-12.3%)	1300.3 (-2.5%)
Thermocouple 2 (K) / Deviation	No heat transfer	910.4 (-17.1%)	974.6 (-10.3%)
	With radiation and conduction	870.0 (-20.8%)	947.5 (-12.8%)
Thermocouple 3 (K) / Deviation	No heat transfer	1063.5 (-4.5%)	1055.0 (-1.4%)
	With radiation and conduction	1009.9 (-9.3%)	1030.7 (-3.7%)

Point 3 has the best accuracy for both models. The overall agreement is verified, once numerical simulation reproduces reasonably the experiments. In point 3, gradients are less severe and the mixing process has a minor role. Distortions are explained by the same flow pattern sensitivity, which is less prominent in this region. It is worth noticing in Fig. 7 that the model accounting for radiation and conduction in the liner under-predicts the temperature in both cases. This indicates that the simulations were conducted consistently.

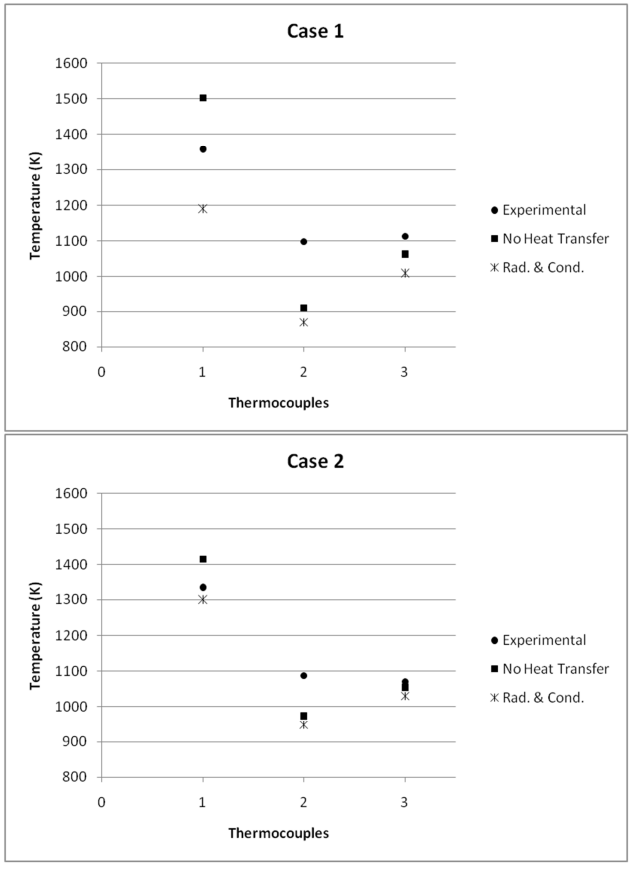

Figure 7. Temperature comparison between experimental results, simulations without heat transfer and simulations with radiation and conduction modeling.

The differences between the two cases cannot be discussed by local points. Case 2 has a slightly lower global equivalence ratio, but it is not plausible to expect lower temperatures in the same points for this reason. The temperature fields depend on much more variables than the equivalence ratio, such as mean distribution of mixture fraction, absolute enthalpy and mixture fraction variance.

Chamber's outlet temperatures were taken to check simulations consistency concerning the energy conservation. The temperature values, presented in Table 4, are the averages of the computational nodes on the outlet plane. The adiabatic flame temperatures at constant pressure, calculated as presented by Turns (2000), for each case according to their global equivalence ratio are also presented in Table 4 (bottom line). Inside the combustion chamber, comparing temperatures to the adiabatic flame temperature does not make sense, because of the different flow statistic (mixture fraction and enthalpy), as previously stated. On the other hand, since the combustion chamber is considered adiabatic, the flow enthalpy should be conserved at the outlet. It is worth keeping in mind, however, that even at the outlet section there are spatial gradients in the mixture fraction and enthalpy, which may lead to deviations from the idealized well mixed reactor model.

Table 4. Chamber outlet temperatures and adiabatic flame temperatures corresponding to the global equivalence ratios (K).

	Cases	
	1	**2**
No heat transfer	1060.2	1040.8
With radiation and conduction	1071.3	1045.3
Adiabatic flame temperature	1104.6	1051.2

As expected, values are very similar. The major discrepancy, 4.0%, relative to the adiabatic flame temperature is observed in Case 1 – No heat Transfer. Small differences are due to the presence of the β-PDF in the CFD simulations model, which differs from the well mixed reactor model used by Turns (2000). Comparing simulations with and without heat transfer, the β-PDFs are different from each other, causing variations between CFD results. Based on these results, one can conclude that the flow enthalpy is conserved and agrees with the experimental data.

Even though the comparison with experimental data is not totally conclusive, there is evidence that heat transfer modeling is necessary to assess the combustion phenomena. Concerning the temperature measurements (Fig. 7), the adherence of simulations with heat transfer is not significantly better than those without it. However, flow structure patterns are changed when considering heat transfer. This pattern is kept in both cases. At measurement stations 2 and 3, both numerical models show temperature below the measured values. Furthermore, as one could expect, simulations considering radiation and conduction inside the liner indicate temperatures below the simulation without these heat transfer processes. At the measurement station 1, where the spatial gradients of all variables are very high, simulations considering radiation and conduction inside the liner show, once again, temperature below the measured values. Simulations without heat transfer have, however, higher values if compared to the measurements. This behavior seems to be inconsistent with the results at the other two measurements points. Concluding, regardless of the lack of more measurements stations in this critical region, it is conservative and logical to assume that the simulation with heat transfer approximates more to the real flow.

Heat transfer modeling has noteworthy effects. As seen in Fig. 5, conduction in the liner is significant and its modeling allows the evaluation of the liner temperature. Simulations indicated that the liner temperature reaches a value around 900 K and this is a valuable estimate that might be used in durability calculations.

Simulations with only radiation modeling and only conduction were performed to have indications regarding the role of each heat transfer form. Figure 8 presents temperature profiles for the four types of simulations performed: no heat transfer, radiation heat transfer, conduction in the liner and both radiation and conduction. The first noticeable characteristic is the temperatures between liner walls and casing. Obviously, only the simulations with conduction have temperatures higher than 300 K in this region. Comparing conduction with and without radiation, one can observe that radiation causes an increase in the casing wall temperature.

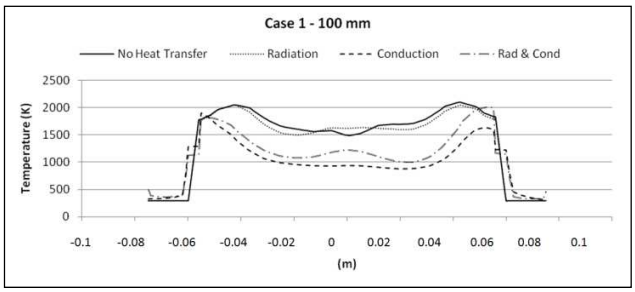

Figure 8. Temperatures of a radial line located 100 mm from the swirler for Case 1.

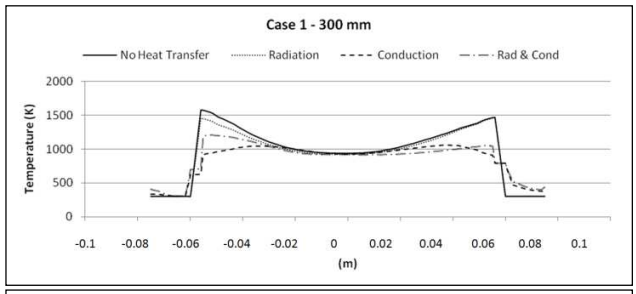

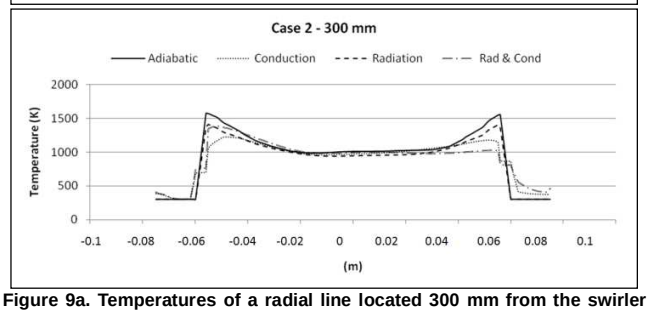

Figure 9a. Temperatures of a radial line located 300 mm from the swirler for both Cases.

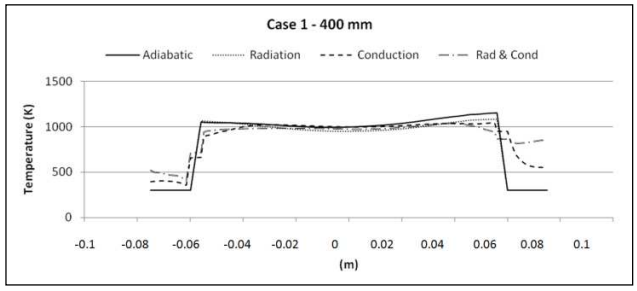

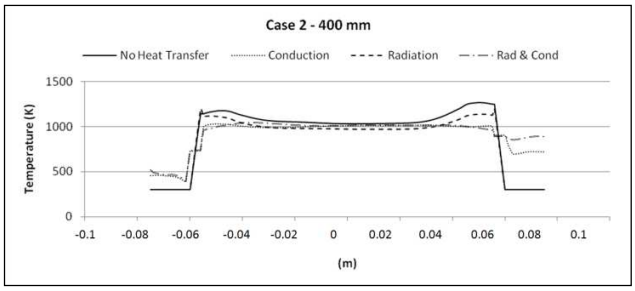

Figure 9b. Temperatures of a radial line located 400 mm from the swirler for both Cases.

Comparing the whole profiles, it is clear that the radiation simulation is more similar to the simulation with no heat transfer, while the conduction simulations (with and without radiation) are similar to each other. It points to a leading role of conduction inside the liner in this chamber. The same tendency is supported in other distances from the swirler for both Cases. Figure 9 shows other two examples. Again, conduction seems to affect more the results. Observing the temperature contours presented in Fig. 5, regardless of the different flow rates, one can see that, in comparison to the no conduction model, there is a temperature increase of ca. 100 – 150 K as the inflow air approaches the swirler. Inflow air heating occurs because of the heat transfer through the liner. Consequently the heated air entering the swirler alters significantly the velocities and mixing processes at the fuel injection region.

Figures 9a and 9b also show an interesting fact: an asymmetry of the region between casing and liner walls at the graphs edges. The air entrance in the casing is made through a manifold inserted asymmetrically, as shown in Fig. 1. This causes the air to achieve higher temperatures in one side of the evaluated line. This characteristic may also be responsible for the slight asymmetry noticed in all the contours shown (Figs. 4 to 6). Comparing Fig. 8 and Fig. 9a and Fig. 9b, one can see, once again, that the region between the fuel injector and the first temperature measurement point is critical. As shown in Fig. 8 there are significant deviations in the temperature profiles not only at the near liner region but also in the whole flow inside the combustor.

The simulations also allowed the evaluation of the swirling flow characteristic. Experiments demonstrated that the chamber stability in the imposed fuel flows was satisfying. This indicated that the swirler was acting at least close to the way it was designed to. Figure 10 shows two tridimensional isosurfaces capable of indicating if the swirling flow is actually being created. On the left is a plot of absolute helicity, which is defined as the dot product between the vorticity vector and the velocity vector. The isosurface value was adjusted manually to provide the best visualization. There are two well defined regions: the first connected to the swirler and the other in the dilution holes region. These two regions have the higher values of absolute helicity, showing high swirling tendency.

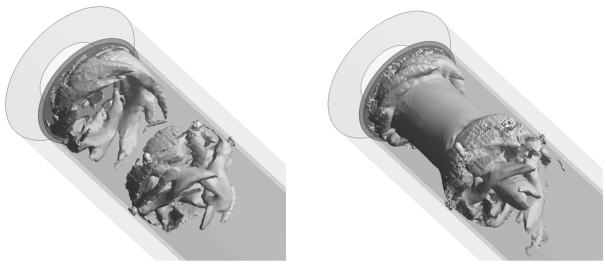

Figure 10. Absolute helicity isosurface (left) and swirling strength isosurface (right) for case 1 with heat transfer simulation.

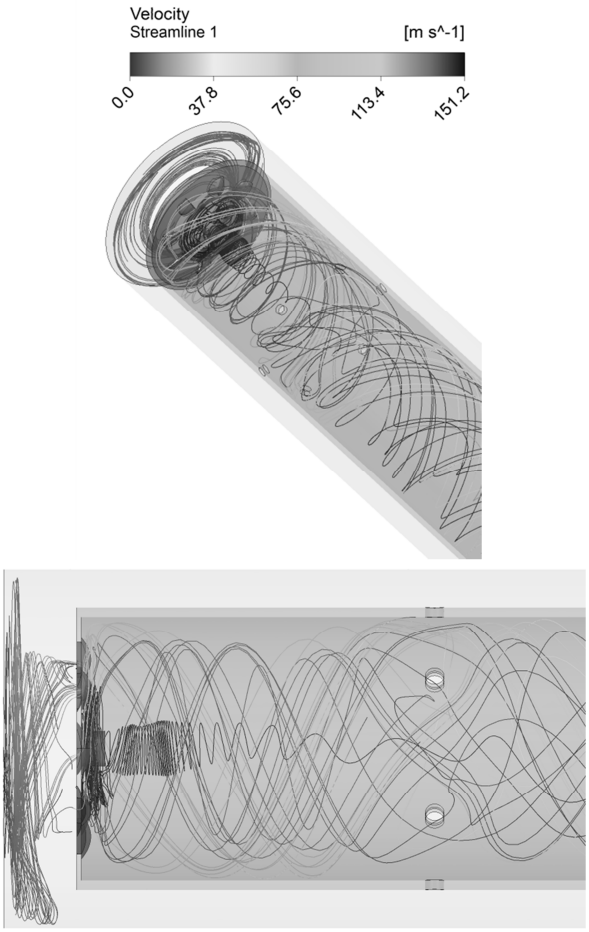

Figure 11. Velocity streamlines seeded on the casing top (gray) and in the fuel inlet (black).

The plot shown on the right of Fig. 10 is an isosurface of swirling strength, which is defined as the imaginary part of the complex eigenvalues of the velocity gradient tensor. This variable is useful to identify helical structures, representing the strength of swirling motion around local centers. Its positive value (as the one highlighted by the isosurface) only appears when there is a local swirling pattern on the flow (Akturk and Camci, 2011).

Therefore, it is likely that the stability found in the experiments is due to the achieved mixing swirling structure. However, as indicated by previous discussions, there is also indication that the mixing process is elongating more than it should. In order to understand why this is happening, the velocity streamlines presented in Fig. 11 are useful.

The gray streamlines were seeded at the top of the chamber's casing, while the black streamlines were seeded in the fuel entrance holes. More than the velocity magnitude, it is interesting to notice the mixing of the two groups of streamlines. A portion of the fuel stays in the center of the chamber, while the mixing occurs mostly close to the liner walls. It is desirable that the fuel is mixed as soon as possible and that the mixing takes place in the center of the chamber.

Consequently, a modification in the swirler geometry may be a way of improving the mixing process. Air should enter closer to chamber's center. On the other hand, such adjustment must be done carefully. It is not recommended to impose more restriction to the air inlet and the swirling flow characteristics must be maintained.

Fuel injection is already made radially. This contributes to the fact that the mixing is mostly located near the walls. Still, modifying this characteristic may elongate even more the mixing process, moving it away from the swirler. Anyhow, injector improvements must be considered.

Conclusions

The present paper reported the design, experimental and computational evaluation of a combustion chamber for a micro-gas turbine fuelled with natural gas. Simulations with four heat transfer models were applied.

The simulations with radiation and liner conduction were considered to better reproduce the flow, since they have a whole different pattern if compared to simulations without heat transfer. In order to verify the consistency of the simulation, comparison of the outlet temperature with the adiabatic flame temperature of a well-mixed reactor is performed. Results show that flow enthalpy is conserved and agrees with experimental data.

Comparison of temperature profiles between different modeling approaches at three planes downstream the fuel injection shows that the region between injection and the first measurement point is critical. The profiles differ in more aspects than just near liner region, having influence on the whole flow inside the combustor.

The analysis of the isolated effects of radiation and liner conduction points to a leading role of liner conduction. Air entering the swirler is heated, leading to significant changes in velocities and mixing process at the fuel injection region.

Other information obtained with the heat transfer model with radiation and conduction inside the liner is its temperature. Simulations indicate that the liner temperature reaches value around 900 K and this estimate might be used in durability calculations for gas turbines combustion chambers.

In order to better support conclusions, more temperature measurements on the region between the fuel injector and point 1 are necessary. This region presents the highest spatial gradients of velocity, mixture fraction and enthalpy considering the whole combustor. The presented results suggest that the flow pattern is quite different depending on the used heat transfer approach. This should be investigated experimentally in more details. Despite the lack of more measurement stations in this critical region, it is conservative and logical to assume that simulations with heat transfer modeling are closer to the real flow.

Flame stability at the investigated flow ratios is achieved by the swirling flow generated by the designed swirler. In addition to the experimental observation of stable operation, simulations show that the swirler in fact increases the mixing processes. However, mixture fraction plots, temperature contours and streamline analysis indicate that the mixing process might still be improved. We suggest modifications to the swirler geometry and/or the fuel injector. Mixing should occur in the center of the chamber and as close as possible to the swirler, being able to improve durability, stability and emissions.

Acknowledgements

This project was supported by FAPESP under the grants 2007/03072-1, 2011/03620-4 and ANP-PRH-19. The authors would like to thank BorgWarner Turbo Systems and Bernauer Ventiladores for their support.

References

Akturk, A. and Camci, C., 2011, “Tip Clearance Investigation of a Ducted Fan Used in VTOL UAVS: Part 2 - Novel Treatments via Computational Design and Their Experimental Verification,” Paper GT 2011-46359, ASME Turbo Expo, Vancouver, Canada, pp 345-357.

Cameretti, M.C., Reale, F. and Tuccillo, R., 2007, “Cycle Optimization and Combustion Analysis in a Low-NOx Micro Gas Turbine”, Journal of Engineering for Gas Turbines and Power, Vol. 129, pp. 994-1003.

Choi, Y.S. and Kang, S.H., 1999, “Application of Through-flow Calculation to Design and Performance Prediction of Centrifugal Compressor”, International Journal of Rotating Machinery, Vol. 5, No. 1, pp. 17-33.

Fluent Inc, 2000. "User´s Guide 5.2", Centerra Park Lebanon, NH, USA.

Ghenai, C., 2010, “Combustion of Syngas Fuel in Gas Turbine Can Combustor”, Advances in Mechanical Engineering, Vol. 2010, Article ID 342357, DOI:10.1155/2010/342357

Kayakol, N., Selçuk, N., Campbell, I. and Gülder, O.L., 2000, “Performance of Discrete Ordinates Method in a Gas Turbine Combustor Simulator”, Experimental Thermal and Fluid Science, Vol. 21, Issues 1–3, pp. 134-141.

Khelil, A., Naji, H., Loukarfi, L., Mompean, G., 2009, “Prediction of a high swirled natural gas diffusion flame using a PDF model”, Fuel, Vol. 88, Issue 2, pp. 374–381.

Kent, J.H. and Honnery, D., 1987, “Soot and Mixture Fraction in Turbulent Diffusion Flames”, Combustion Science and Technololy, Vol. 54, Issue 1-6, pages 383-398, DOI: 10.1080/00102208708947062.

Lefebvre, A.H. and Ballal, D.R., 2010, “Gas Turbine Combustion: Alternative Fuels and Emissions”, Taylor & Francis Group, Philadelphia, USA, 537 p.

Modest, M.F., 2003, “Radiative Heat Transfer”, Elsevier Science, San Diego, USA, 822 p.

Palm, R., Grundmann, S., Weismüller, M., Šarić, S., Jakirlić, S. and Tropea, C., 2006, “Experimental Characterization and Modeling of Inflow Conditions for a Gas Turbine Swirl Combustor”, International Journal of Heat and Fluid Flow, Vol. 27, pp. 924-936.

Piro, M. H., 2007,“ Experimental and Numerical Investigations of Velocity and Turbulent Quantities of a Jet Diffusion Flame”, 2007, Master of Science (Engineering) Thesis, Department of Mechanical and Materials Engineering, Queen’s University Kingston, Ontario, Canada.

Sacomano Filho, F. L., 2011, “Simulações de chamas turbulentas de etanol com modelo de turbulência k-ε” [online], Master of Science (Engineering) Thesis, Escola Politécnica, Universidade de São Paulo, Sao Paulo, Brazil.

Tomczak, H-J., Benelli, G., Carrai, L. and Cecchini, D., 2002, “Investigation of a Gas Turbine Combustion System Fired with Mitures of Natural Gas and Hydrogen”, IFRF Combustion Journal, Article Number 200207, ISSN 1562-479X.

Tuccillo, R. and Cameretti, M.C., 2005, “Combustors and Combustion for MGT Applications”, Educations Notes RTO-EN-AVT131, Paper 5, Neuilly-sur-Seine, France, pp. 1-56.

Turns, S.R., 2000, “An Introduction to Combustion: Concepts and Applications”, McGraw-Hill, ISBN-13: 978-0073380193

Weber, R., Visser, B.M. and Boysan, F., 1990, “Assessment of Turbulence Modeling for Engineering Prediction of Swirling Vortices in the Near Burner Zone”, International Journal of Heat and Fluid Flow, Vol. 11, No. 3, pp. 225-235.

Xia, J.L., Yadigaroglu, G., Liu, Y.S., Schmidli, J. and Smith, B.L., 1998, “Numerical and Experimental Study of Swirling Flow in a Model Combustor”, International Journal of Heat and Mass Transfer, Vol. 41, No. 11, pp. 1485-1497.